Published in final edited form as:
Nat Neurosci. 2018 July ; 21(7): 932–940. doi:10.1038/s41593-018-0168-3.

Direct pericyte-to-neuron reprogramming via unfolding of a neural stem cell-like program

Marisa Karow[#1,2,§], **J. Gray Camp**[#3], **Sven Falk**[2,4], **Tobias Gerber**[3], **Abhijeet Pataskar**[5], **Malgorzata Gac-Santel**[3], **Jorge Kageyama**[3], **Agnieska Brazovskaja**[3], **Angela Garding**[5], **Wenqiang Fan**[1], **Therese Riedemann**[2], **Antonella Casamassa**[1,13], **Andrej Smiyakin**[6], **Christian Schichor**[7], **Magdalena Götz**[2,4], **Vijay K. Tiwari**[5], **Barbara Treutlein**[#3,8,9,§], and **Benedikt Berninger**[#1,10,11,12,§]

[1]Institute of Physiological Chemistry, University Medical Center Johannes Gutenberg University Mainz, Mainz, Germany

[2]Physiological Genomics, Biomedical Center, Ludwig Maximilians University Munich, Planegg/Martinsried, Germany

[3]Max Planck Institute for Evolutionary Anthropology, Leipzig, Germany

[4]Institute for Stem Cell Research, Helmholtz Center Munich, German Research Center for Environmental Health, Neuherberg, Germany

[5]Institute of Molecular Biology (IMB), Mainz, Germany

[6]Miltenyi Biotec GmbH, Bergisch Gladbach, Germany

[7]Department of Neurosurgery, Ludwig Maximilians University, Munich, Germany

[8]Max Planck Institute of Molecular Cell Biology and Genetics, Dresden, Germany

[9]Technical University Munich, Munich, Germany

[10]Focus Program Translational Neuroscience, Johannes Gutenberg University Mainz, Mainz, Germany

[§]**Correspondence should go to:** Correspondence and requests for materials and data should be addressed to M.K. (marisa.karow@med.uni-muenchen.de), and B.T. (barbara_treutlein@eva.mpg.de), and B.B. (berningb@uni-mainz.de).
[13]Present address: Division of Pharmacology, School of Medicine, "Federico II" University of Naples, Naples, Italy.

Data availability and accession codes

The scRNA-seq data used in this study have been in the Gene Expression Omnibus (GEO) under accession number GSE113036. The data that support the findings of this study are available from the corresponding author upon reasonable request.

Author contributions

M.K, J.G.C., B.T., and B.B. conceived the study and designed experiments; M.K. performed direct reprogramming experiments; M.K., S.F., A.P., and V.K.T. performed analysis of bulk RNA-seq data; A.B. helped with processing of the 10xGenomics data; A.G. performed RNA-isolation for bulk RNA-seq analysis; W.F. performed time-lapse imaging experiments; T.R. performed electrophysiological recordings; A.C. performed Sholl analyses; A.S. performed immunocytochemical analyses; C.S. provided human brain biopsies; M.G. provided material; J.G.C., M.Ga., and T.G. performed single-cell RNA-seq experiments and sequenced libraries; J.G.C., J.K., and B.T. analyzed single-cell RNA-seq data; all authors discussed the data; M.K., J.G.C., S.F., B.T., and B.B. wrote the paper.

Competing financial interests

The authors declare no competing financial interests.

Europe PMC Funders Author Manuscripts

[11]Centre for Developmental Neurobiology, Institute of Psychiatry, Psychology & Neuroscience, King's College London, London, UK

[12]MRC Centre for Neurodevelopmental Disorders, Institute of Psychiatry, Psychology & Neuroscience, King's College London, London, UK

[#] These authors contributed equally to this work.

Abstract

Ectopic expression of defined transcription factors can force direct cell fate conversion from one lineage to another in the absence of cell division. Several transcription factor cocktails have enabled successful reprogramming of various somatic cell types into induced neurons (iNs) of distinct neurotransmitter phenotype. However, the nature of the intermediate states that drive the reprogramming trajectory towards distinct iN types is largely unknown. Here we show that successful direct reprogramming of adult human brain pericytes into functional iNs by Ascl1 and Sox2 (AS) encompasses transient activation of a neural stem cell-like gene expression program that precedes bifurcation into distinct neuronal lineages. Intriguingly, during this transient state key signaling components relevant for neural induction and neural stem cell maintenance are regulated and functionally contribute to iN reprogramming and maturation. Thus, AS-mediated reprogramming into a broad spectrum of iN types involves the unfolding of a developmental program via neural stem cell-like intermediates.

Introduction

Direct lineage reprogramming is an emerging strategy to harness cellular plasticity of differentiated cells for lineage conversion into desired target cell types for disease modeling and tissue repair[1–4]. While direct lineage reprogramming from starting to target cell type classically occurs without cell division, thereby sharply contrasting reprogramming towards induced pluripotency[5], little is known about the intermediate states that bridge the trajectory between start and end points. Two models have been proposed according to which direct reprogramming is mediated either through direct conversion between fully differentiated states or reversal to a developmentally immature state[6]. Furthermore, reprogramming efficiency and final differentiation outcomes are highly cellular context-dependent, for which the underlying reasons are only incompletely understood[7,8]. Analyses of the transcriptome alterations induced by the reprogramming factors has yielded fundamental insights into the molecular mechanisms of iN conversion[9–12]. For instance, a single factor Ascl1 can reprogram mouse astrocytes into induced neurons (iN) with high efficiency[13], while the same factor induces a muscle cell-like fate in mouse embryonic fibroblasts (MEF) alongside neuronal fates[11,14]. Efficient reprogramming of MEFs into iNs requires co-expression of additional factors (e.g. Brn2, Ascl1, Myt1l; BAM)[9,11,12,15]. Moreover, Ascl1 induces a GABAergic neuron identity in mouse astrocytes[10,13], while BAM-transduced fibroblasts predominantly adopt a glutamatergic phenotype[15], raising questions of how the respective reprogramming trajectories translate into distinct iN transmitter and subtype identities.

In the present study, by analyzing transcriptomes at population and single cell level we aimed at reconstructing the trajectories that underlie direct lineage conversion of adult human brain pericytes into induced neurons (iNs) by forced expression of Ascl1 and Sox2 (AS)16. This allowed us to scrutinize the contribution of the starting cell population heterogeneity to the variability in reprogramming success. By identifying cells of distinct reprogramming competence, we were able to reconstruct a trajectory of productive AS-mediated iN generation, allowing us to uncover intermediate states during successful conversion. Surprisingly, we found that despite the absence of cell division, cells in the productive trajectory passed through a neural stem cell-like state. Transiently induced genes, many of which are core components of signaling pathways, typified this intermediate state, and interference with these signaling pathways demonstrated their functional importance for the reprogramming process. Finally, the productive reprogramming trajectory revealed an unexpected point of bifurcation into lineages whose transcriptomes were dominated by transcription factor families involved in the specification of GABAergic and glutamatergic subclasses of forebrain neurons.

Results

Ascl1 and Sox2 synergism in inducing neuronal gene expression in pericytes

We have recently shown that adult human brain pericytes can be reprogrammed into iNs via forced expression of the transcription factors Ascl1 and Sox2 (AS), and time-lapse imaging showed that this conversion occurs in the absence of cell division qualifying it as direct lineage reprogramming16. Given that adult human brain pericyte reprogramming into functional iNs requires co-expression of Sox2 alongside Ascl116, we first addressed the contribution of each factor individually or in combination to the gene expression programs underlying pericyte-to-neuron conversion (Fig. 1a, b). We performed RNA-seq of early-passage cultured human brain pericytes obtained from 3 different adult donors transduced with retroviruses encoding a reporter for control, *Ascl1, Sox2*, or *Ascl1* plus *Sox2* (AS) at early stages (2 days post infection (dpi) and 7 dpi) of reprogramming (Fig. 1a). Surprisingly, Sox2 only induced minor changes in gene expression, both at 2 and 7 dpi (Fig. 1c and Supplementary Fig. 1a, e and Supplementary Table 1). In contrast, Ascl1 and AS substantially altered gene expression at both stages (Fig. 1c and Supplementary Fig. 1a, e, f). Intriguingly, Ascl1 and AS changed the expression of distinct sets of genes. We noticed that several of the Ascl1-only altered genes are expressed in cells of the mesodermal lineage, indicative of a failure of crossing the lineage barrier towards neurogenesis. In sharp contrast, AS resulted in significant induction of genes related to neurogenesis (Fig. 1d and Supplementary Fig. 1e, f and Supplementary Table 1). Moreover, we detected upregulation of several transcription factors and non-coding RNAs playing key roles in forebrain GABAergic neurogenesis17,18 (Fig. 1d and Supplementary Fig. 1e, f and Supplementary Table 1,2). Yet, we also observed a significant increase in *NEUROG2* expression (Fig. 1d), which is associated with diverse excitatory neuron identities.

Comparison of the genes upregulated by Ascl1-only or AS with those transactivated by Ascl1 in mouse neural stem cells19 revealed a progressive induction of direct Ascl1 neural stem cell target genes between dpi 2 and 7 (Supplementary Fig. 1b and Supplementary Table

3). However, many of the direct Ascl1 neural stem cell target genes became induced only upon co-expression of Sox2 (Supplementary Fig. 1c, d), indicating that the proposed on-target pioneer factor activity of Ascl19,19 is highly context-dependent.

To further dissect the differences in the early gene expression programs induced by Ascl1 or AS, we measured 280 single cell transcriptomes of Ascl1- (146) and AS-expressing (134) cells by single-cell RNA-seq at dpi 2 and 7. Principal component analysis (PCA) followed by t-stochastic neighbor embedding (tSNE) of single cell transcriptomes revealed an early and progressive separation of Ascl1-only and AS-expressing cells (Fig. 1e). Pericyte identity genes (e.g. *PDGFRB, COL1A1, CAV1*) became downregulated in Ascl1- and AS-expressing cells (Supplementary Fig. 1g), but only the latter acquired a GABAergic neuron (iGN) fate signature (*DLX1/2, DLX5/6, SATB1* etc.) (Fig. 1e and Supplementary Fig. 1h). In agreement with our bulk RNA-seq data and published data from MEF-to-neuron reprogramming11 Ascl1-expressing cells induced myocyte differentiation genes (e.g. *MUSTN1*) (Supplementary Fig. 1h). Occasionally individual AS cell transcriptomes clustered with those of Ascl1-only cells suggesting failed AS synergism as a potential mechanism underlying reprogramming failure (Fig. 1f). Overall, these data demonstrate that Ascl1 alone is unable to induce a neuronal program in adult human brain pericytes but requires synergism with Sox2.

Pericyte heterogeneity and reprogramming competence

To define the competence of adult human brain pericytes for AS-induced reprogramming, we next compared the transcriptomes of control pericytes with those of AS-transduced cells at early and later stages of reprogramming. To our surprise, t-SNE analysis revealed that control cells fell into two discernible clusters (Fig. 2a, b and Supplementary Fig. 2a, b), here referred to as group 1 and group 2 pericytes, with differentially enriched GO terms (Supplementary Fig. 2c and Supplementary Table 4). While both groups highly expressed several classical pericyte genes (i.e., *PDGFRB, CAV1, DCN* etc.) (Fig. 2a and Supplementary Fig. 2b), other pericyte-associated genes such as *ANGPT1*, *APOE*, and *LEPR* were differentially expressed (Supplementary Fig. 2a, b) and such differential expression could be confirmed on protein level (Fig. 2c, f and Supplementary Fig. 2d). Intriguingly, transcriptomes of AS-transduced cells exhibited distinct degrees of relatedness to the two pericyte starting populations, with cells undergoing successful reprogramming being more similar to group 2 pericytes (Fig. 2d, e). This data strongly suggest that the two pericyte groups differ markedly in their response to AS. In fact, t-SNE analysis indicated that productive reprogramming towards neurogenesis originated specifically from group 2 pericytes (Fig. 2a, e). In contrast, group 1 pericytes appear to give rise to a distinct population positive for the hypothalamic neuronal marker PMCH but lacking expression of other neuronal genes which thus precluded identifying these cells as hypothalamic neurons (Fig. 2a). Besides AS-transduced cells clustering differentially with group 1 and group 2 pericytes, we observed two smaller clusters of AS-transduced cells enriched in genes involved in cell cycle progression (e.g. *MKI67*) and potentially an alternative fate marked by the expression of *POU2F3*. To independently corroborate differential neurogenic competence of group 1 and group 2 pericytes we FACS-purified these populations via antibodies specific to leptin receptor, encoded by the *LEPR* gene (Fig. 2f, g and

Supplementary Fig. 2d). Consistent with the observation that iNs may originate from group 2 pericytes, we found that leptin receptor-negative cells are more prone to undergo AS-induced neurogenesis than leptin receptor-positive cells (Fig. 2h). This data provide experimental evidence that the two pericyte starter populations display distinct degrees of reprogramming competence.

Transient activation of a neural stem cell-like program

We next reconstructed the transcriptome trajectory of reprogramming-competent pericytes into iNs by pseudotemporal ordering20 (Fig. 3a). Genes that mark pericyte identity such as *PDGFRB*, *CAV1*, and *CFH* became gradually downregulated. Conversely, genes associated with the acquisition of a neuronal fate were progressively upregulated with more linear (e.g. *CHD7*, *DLX5*) or non-linear dynamics (*SNAP25*) (Fig. 3b, c), possibly reflecting distinct gene expression waves during early and later phases of neuronal differentiation. Most intriguingly, we identified a set of genes, which became upregulated early during the reprogramming process, but then declined again as neuronal differentiation progressed (Fig. 3b, c). We refer to these genes as switch genes. These include genes involved in the regulation of cell signaling such as *NOG*, *LEFTY2*, *DKK1*, and *NOTCH2* suggesting that modulation of signaling pathways is important during early phases of productive reprogramming (see below). The conspicuous dynamics of the regulation of these genes urged us to interrogate their expression during mouse embryonic development. Intriguingly, the switch genes were markedly enriched in the germinal zones of the developing CNS containing the neural stem cells (Fig. 3d and Supplementary Fig. 3a). This strongly suggests that cells undergoing productive reprogramming by AS transiently acquire a neural stem cell-like state. This was further corroborated when analyzing the expression levels of these genes in human fetal brain tissue21 with higher levels of expression being found in distinct human neural stem cells (i.e. apical radial glia, aRG and basal radial glia, bRG) as compared to neurons (Fig. 3e). Consistent with the upregulation of the switch genes during successful reprogramming, mapping the switch gene signature onto the tSNE plot shown in Fig. 2a revealed its specific occurrence in the cell population that connects productive group 2 pericytes with iNs (Fig. 3f). In contrast, the switch gene signature was absent from transcriptomes of AS-transduced cells in the immediate neighborhood of group 1 pericytes (Fig. 3f), indicating that acquisition of a neural stem cell like-state is critical for AS-mediated pericyte-to-iN reprogramming. Of note, mapping the same switch gene signature onto previously published single cell transcriptomes undergoing MEF-to-iN reprogramming11 revealed a surprisingly high base level of switch gene expression in the MEF starting population, and its expression did not increase at any stage along the MEF-to-neuron axis but was found to be strongly decreased in neurons (Supplementary Fig. 3b). These data are indicative of fundamental differences in the reprogramming trajectories of these two distinct reprogramming paradigms. Intriguingly, time-lapse imaging of pericytes during AS reprogramming revealed the occurrence of different cellular morphologies: while at early phases of reprogramming cells displayed a flat fibroblast-like morphology, at subsequent phases processes undergoing dynamic turn-over akin to multipolar progenitors appeared (Fig. 3g and Supplementary Movie 1). Finally, at the end of the reprogramming process, neuron-like cells dramatically decreased their motility and protruded processes of

increased stability. Thus, the cellular behavior and morphology are consistent with the notion of distinct cellular states underlying the reprogramming of pericytes into iNs.

Modulation of signaling pathways

The conspicuous regulation of several components of signaling pathways, well known to play key roles during neural induction and neural stem cell maintenance22, such as of the BMP inhibitor *NOG*, the ACTIVIN/NODAL inhibitor *LEFTY2*, as well as *NOTCH2* and its downstream targets *HEY1* and *ID1*, prompted us to investigate whether these pathways are of functional importance for successful reprogramming. To test the importance of modulation of NODAL and BMP signaling, we treated pericytes during early phases of reprogramming with recombinant NODAL (1 μg/ml) and BMP4 (30 ng/ml) (Fig. 4a, b). These treatments resulted in a significant reduction of reprogramming as determined by the number of TUBB3-positive cells amongst AS-transduced cells (Fig. 4c). Conversely, inhibition of BMP, ACTIVIN/NODAL, and TGF-β signaling via the small molecules Dorsomorphin (1 μM) and SB431542 (10 μM) caused a 3-fold increase in the number of reprogrammed iNs (Fig. 4d, e). To address the relevance of NOTCH signaling in the reprogramming process we treated AS-transduced pericytes with the γ-secretase inhibitor N-[N-(3,5-Difluorophenacetyl)-L-alanyl]-S-phenylglycine t-butyl ester (DAPT). DAPT treatment (10 μM) resulted in a marked increase in the number of iNs (Fig. 4d, e). This finding is consistent with the role of Notch signaling in inhibition of neurogenesis and neural stem cell maintenance23.

Though AS induction leads to productive iN reprogramming, we observed that maturation seems to stall at dpi 14, either because cells at later time points failed to mature further or because of a technical bias against harvesting healthy iNs at later stages (Fig. 3a). Our data showed that productive reprogramming involves inhibition of BMP signaling, and blocking BMP signaling appeared to promote maturation as suggested by an increased morphological iN complexity (Fig. 4e). We therefore analyzed the effect of the BMP inhibitor Dorsomorphin during early phases of the reprogramming process on subsequent neuronal maturation (Fig. 5a). Dorsomorphin-treated AS-induced neurons exhibited a markedly increased morphological complexity and soma size (Fig. 5b,c and Supplementary Fig. 4a), as well as increased membrane capacitance and decreased membrane resistance (Fig. 5d and Supplementary Fig. 4b). scRNA-seq on Dorsomorphin-treated AS-induced neurons revealed that genes associated with synapse formation and synaptic function showed increased expression relative to untreated AS transduced cells (Fig. 5e). In line with enhanced iN maturation we also noted enhanced GABA and PVALB immunoreactivity (Supplementary Fig. 4c).

Bifurcation into distinct iN lineages

This data urged us to have a closer look at the neuronal subtype specification induced by AS with or without Dorsomorphin (ASD). We focused on iNs that expressed both *SNAP25* and *MAP2* and analyzed 20 AS and 72 ASD cells. The majority of AS and ASD iNs exhibited a forebrain GABAergic interneuron program characterized by coordinated expression of multiple members of the *DLX* gene family (Fig. 5f). Intriguingly we found evidence for further sub-specification among the *DLX*-expressing iNs. We observed distinct clusters of

VIP-expressing neurons some of which also co-expressed *CCK*. Likewise we noted two clusters expressing specifically *SST* (Fig. 5f).

However, we also noted a subset of iNs that expressed a transcription factor of the glutamatergic lineage, *NEUROG2*. Intriguingly, these iNs also expressed downstream targets *NEUROD1* and *NEUROD4*, consistent with the expression of a telencephalic glutamatergic neuron program10,24. The fact that this subset also expressed RELN (Fig. 5f) may indicate that these iNs acquire a Cajal-Retzius neuron-like program. It is noteworthy that while the majority of *DLX1*-expressing cells were *NEUROG2* negative and many high *NEUROG2*-expressing cells were *DLX1* negative, we observed some outliers expressing both genes (Supplementary Fig. 4d). This may reflect the possibility that the definitive decision between the two major neuron lineages (GABA versus glutamate) had not yet taken place in these cells. To reveal the developmental trajectory towards a *DLX*- or *NEUROG2*-dominated fate, we employed pseudotemporal ordering of the transcriptomes of AS cells of the productive path and d14 ASD cells. Intriguingly, we observed a bifurcation of the trajectory into a *DLX*- and *NEUROG2*-dominated path, which preceded neuronal differentiation marked by *SNAP25* expression (Fig. 5g and Supplementary Fig. 4e). Projecting the switch gene signature identified in Fig. 3c onto the reprogramming path revealed that the transient expression of neural stem cell-like genes occurs and ceases prior to lineage bifurcation (Fig. 5h). Consistent with the increased maturation of ASD cells, the distribution of ASD transcriptomes was shifted farther along the trajectory of pericyte-to-iN reprogramming (Fig. 5i). We corroborated the emergence of *DLX*- or *NEUROG2*-expressing inhibitory and excitatory neuronal lineages using an alternative scRNA-seq method and a second pericyte donor (Supplementary Fig. 5).

To test whether NEUROG2 indeed suffices to induce a glutamatergic phenotype we overexpressed *NEUROG2* alongside AS (ASN) (Supplementary Fig. 4f). NEUROG2 overexpression resulted in the almost complete suppression of *DLX2* (Fig. 5j), suggesting that NEUROG2 can divert iNs from adopting predominantly a GABAergic phenotype towards generating mostly glutamatergic neurons. Accordingly, we found that ASN neurons exhibited vesicular glutamate transporter immunoreactivity (Supplementary Fig. 4g).

Discussion

In the present study, we have shown that reprogramming success of adult human brain pericytes into iNs by the transcription factors Ascl1 and Sox2 (AS) critically depends on cellular context as revealed by the observation that pericyte heterogeneity is a key determinant for reprogramming competence. Successful reprogramming by AS encompasses the passage through a neural stem cell-like intermediate state, yet it occurs in the absence of cell division. Moreover, regulation of signaling pathways during the neural stem cell-like state was of functional importance for the reprogramming outcome. This data indicates that AS-mediated reprogramming involves the unfolding of developmental programs and argues for the engagement of hierarchical developmental gene regulatory networks6 rather than direct interconversion between two states of terminal differentiation. Finally, we found that following the transition through a neural stem cell-like state the reprogramming trajectory eventually bifurcates to give rise to two distinct branches characterized by *DLX*- and

NEUROG-dominated gene expression and indicative of bifurcation into GABAergic and glutamatergic lineages. This provides a mechanistic explanation for the common observation that one and the same reprogramming cocktail can yield neurons of distinct neurotransmitter phenotypes15,25.

We observed that reprogramming competence of adult human brain pericytes is highly variable and a main source for this variability is pericyte heterogeneity. Heterogeneity of pericytes has been described in many tissues and may reflect distinct embryonic origins26. Our scRNA-seq experiments revealed two distinct populations, of which one, characterized by high *LEPR* expression, displayed markedly reduced reprogramming propensity. Intriguingly, using scRNA-seq a recent study showed that several of the heterogeneously expressed genes are also expressed at highly variable levels in acutely isolated human midbrain pericytes27, which might indicate that similar heterogeneity occurs in vivo. However, our study may actually underestimate overall pericyte heterogeneity, as we included in our scRNA-seq analysis only retrovirus-transduced cells, for which ongoing cell division at the time of transduction is required. We would also expect that proliferative pericytes do not perfectly match pericytes under resting conditions, but may be more akin to those found to undergo cell division in response to severe CNS injury28.

Revealing the cell context requirements for reprogramming is of greatest importance if direct lineage reprogramming is to be of therapeutic value. Many reprogramming factor cocktails that work well with mouse cells (e.g. MEFs) are rather inefficient with human cells, and in particular, when of adult tissue origin. It will be therefore a fruitful field of investigation to identify besides transcriptome differences, also disparities in the epigenome between the two subpopulations of pericytes identified here. This may yield potential molecular targets for improved reprogramming strategies that may apply to other adult human somatic cell types.

A key finding of our study is the observation that AS transduced cells pass through a neural stem cell-like state prior to differentiating into iNs. This neural stem cell-like state is characterized by expression of a battery of genes that are normally expressed in neural stem or progenitor cells during forebrain embryonic development, to which we referred here as switch genes as they are dynamically regulated during the reprogramming process. While referring to the state characterized by switch gene expression to a neural stem cell-like state, we do not equate it to a bona fide neural stem cell state. This distinction is warranted given the absence of classical markers of neural stem cells such as *MSI1* (Musashi) or *NES* (Nestin) during the switch state, some anomalies in gene regulation such as *DLX5* preceding *DLX1* expression in time, and above all the absence of cell division and of a transcriptomic signature of an active cell cycle. We hypothesize that genes induced during the switch state represent a neural stem cell gene expression module specifically regulated by Ascl1 and Sox2, and other transcription factors may be required for inducing other neural stem cell markers. Importantly, the AS-induced neural stem cell expression module appears to be sufficient to drive the trajectory towards neuronal differentiation.

Switch genes include components of several signaling pathways such as the ACTIVIN/NODAL (*LEFTY2*), BMP (*NOG*), and NOTCH (*HES5, HEY1, ID1, NOTCH2*) signaling

pathways. By activating or inhibiting the ACTIVIN/NODAL and BMP pathways during the early phase of reprogramming through recombinant ligands or pharmacologically, we could show that these pathways exert an important influence on reprogramming efficiency. The fact that inhibition of ACTIVIN/NODAL and BMP signaling is required for reprogramming is consistent with the fact that inhibition of these pathways is important for neural induction during embryonic development22, can be utilized for driving human pluripotent stem cells towards neural lineages29, and enhances transcription factor-mediated reprogramming25,30. Most intriguingly, we found that inhibition of NOTCH signaling promoted reprogramming. This is consistent with the role of NOTCH signaling in preventing neuronal differentiation of neural stem cells31. The conspicuous induction of the NOTCH ligand *DLL1* during reprogramming suggests that *DLL1*-expressing cells exert a differentiation inhibitory effect on other AS-transduced cells, an inhibition, which can be relieved pharmacologically. Intriguingly, iNs appear to express Myt1, which has recently reported to be induced cell-autonomously by Ascl1 and to repress Notch signaling32. Likewise, its close relative Myt1l, a widely used component of the BAM reprogramming cocktail has been shown to repress Notch signaling12. This suggests that the BAM cocktail exhibits similarities to AS' mechanism of reprogramming, however that the addition of the postmitotic repressor Myt1l serves to curtail molecular pathways of the switch state that keep neuronal differentiation in check.

Another intriguing aspect of *NOTCH2* expression during reprogramming is the fact that Notch2, has been recently described to repress cell cycle-related genes and drive neural stem cells to quiescence, which may account in part for the lack of cell division during the switch state33.

Surprisingly, we found that human brain pericytes reprogrammed by AS undergo bifurcation into lineages dominated by transcription factors that specify inhibitory and excitatory neuron fates. This bifurcation was corroborated using two distinct scRNA-seq platforms (Fluidgm C1, 10x Genomics). While the *DLX* gene family dominated branch was enriched for genes characteristic for the GABAergic neuron lineage (e.g. *GAD1, GAD2*), the *NEUROG*-expressing branch expressed other transcription factors of the glutamatergic neuron lineage such as *NEUROD1* and *NEUROD4*. Moreover, cells of the latter lineage also expressed *RELN,* suggesting similarities to Cajal-Retzius subtype of glutamatergic neurons. The fact that forced expression of *Neurog2* in AS-transduced pericytes suppresses *DLX* gene expression may indicate that lineage bifurcation is driven by mutual cross-repression of *NEUROG* and *DLX* family genes. Our data raise the intriguing possibility that the bi-potent neural stem cell-like state observed during AS reprogramming relates to the suggested common precursor generating both, glutamatergic and GABAergic neurons in the cerebral cortex of human and non-human primates34.

Overall, our study not only provides new insights into the biology underlying iN reprogramming, but also sheds light on the capacity of two transcription factors Ascl1 and Sox2 to cooperate in the generation of diverse neuronal subtypes, a cooperation that may be relevant during human brain development. The identification of the molecular programs that establish cellular intermediates and lineage bifurcations during iN reprogramming provides

handles to improve lineage conversion of human brain-resident cells towards therapeutically relevant cell types.

Online Methods

Culture of primary human pericytes

Primary pericytes were derived as described previously from adult human brain tissue16,35. Briefly, specimens of cerebral cortex were obtained from standard surgical interventions of patients aged between 19-70 years of both sexes. The study was approved by the ethical committee of the Medical Faculty of the LMU Munich and written informed consent was obtained from all patients. Human tissue was enzymatically (TrypLE, Life technologies) and mechanically dissociated and following centrifugation at 1000 rpm for 5 minutes and resuspension in pericyte medium, cells were plated in T75 cell culture flasks. Pericyte growth medium consisted of DMEM high glucose with GlutaMAX, 20% FBS, and penicillin/streptomycin. Medium was changed twice per week and subcultivation at a ratio of 1:3 was performed every 10 - 14 days. Cells were grown under low oxygen conditions (5% O_2, 5% CO_2) (Galaxy 170R, New Brunswick).

Retroviral transduction and treatments of human pericytes

The retroviral backbone used for lineage conversion of pericytes into iNs allowed for the polycistronic expression of *Ascl1* and *Sox2* (connected via p2A) under the control of an internal chicken beta-actin promoter with cytomegalovirus enhancer (CAG) together with either *DsRed* or *GFP* downstream of an internal ribosomal entry site (IRES). For control, cultures were transduced with a virus encoding only *DsRed* or *GFP* behind an IRES site as described previously13,16.

Retroviral transduction of primary pericyte cultures was performed 24 h after plating on either Poly-D-lysine coated glass coverslips or T25 or T75 cell culture flasks without coating, using VSV-G (vesicular stomatitis virus glycoprotein)-pseudotyped retroviruses encoding neurogenic fate determinants as described previously16,35. Samples (pericyte donors, coverslips in 24-well plates, T25 or T75 cell culture flasks) were randomly assigned for transduction with different viruses. 24 hours after transduction, the medium was replaced by a differentiation medium consisting of DMEM high glucose with GlutaMAX and B27 supplement (Gibco). In case of growth factor or small molecule treatments, addition was performed on day 1, 3, and 5 following transduction. Factors were added to a final concentration of 1 μM 30,36 for Dorsomorphin (Sigma-Aldrich); 10 μM for DAPT (N-[N-(3,5-Difluorophenacetyl)-L-alanyl]-S-phenylglycine t-butyl ester; Stem Cell Technologies); 10 μM 37,38 for SB431542 (Stem Cell Technologies); 30 ng/ml 39,40 for recombinant human BMP4 (Preprotech); 1 μg/ml 41,42 for recombinant human NODAL (RnD Systems). Cells were allowed to differentiate under low oxygen conditions (5% O_2, 5% CO_2). Reprogramming efficiency was calculated by quantifying TUBB3-immunoreactive cells out of reporter-positive transduced cells 3-5 weeks following transduction with retroviruses.

Europe PMC Funders Author Manuscripts

Fluorescence-activated cell sorting (FACS)

For sorting of transduced cells for further i) culturing, ii) bulk RNA-sequencing, iii) scRNA-sequencing, primary pericytes were detached from the culture dish using TrypLE for 4-6 minutes and subsequently resuspended in 500-1000 µl pericyte growth medium. Cell sorting was performed by taking advantage of the combined expression of Ascl1-Sox2 with a fluorescent reporter protein (either DsRed or GFP). Gating was achieved via subtracting the autofluorescence of non transduced cells and control (DsRed or GFP only) transduced cells were used as respective controls. Following sorting, cells were i) collected in pericyte growth medium and plated on PDL-coated glass cover slips on 24-well plates for further culturing, ii) directly collected into RLT buffer (Qiagen) and stored at -80°C until RNA isolation for bulk RNA-seq, or iii) prepared for single cell loading onto C1 fluidigm chip for scRNA-seq. For the separation of LEPR-positive and -negative pericyte populations, pericyte cultures were detached from the culture dish using TrypLE for 4-6 minutes and subsequently 1-5 x 10^5 cells were resuspended in 100 µl staining solution (PBS plus 0.5% BSA). Primary antibody (Alexa647-conjugated CD295 (LEPR) (1:20, BD Pharmingen, cat.no. 564376) was added and cells were incubated for 30 min on ice in the dark. After washing three times in staining solution, cells were resuspended in 500 µl pericyte growth medium and subjected to cell sorting using a FACS Aria (BD). An Alexa647-conjugated isotype control antibody (1:100, BD Pharmingen) was used to gate the proper populations.

Immunohistochemical staining

Cell cultures were fixed in 4% paraformaldehyde (PFA) in phosphate buffered saline (PBS) for 15 min at room temperature. Cells were first pre-treated in blocking solution consisting of 0.2 - 0.5% Triton X-100 and 10% donkey serum in PBS for 60 min, followed by incubation with the primary antibodies in 100 µl in the same solution for 1 h at room temperature or overnight at 4°C. After extensive washing in PBS, cells were incubated in the same solution with appropriate species- or subclass-specific secondary antibodies conjugated to fluorophores. Coverslips were finally mounted onto a glass slide with an anti-fading mounting medium (Aqua Poly/Mount; Polysciences, Warrington, PA). For multidimensional immunofluorescence staining, fixed cell cultures were subjected to sequential immunofluorescence staining/destaining cycles adapted from a technique published by Schubert et al.43.

Microscopy and time-lapse imaging

Immunocytochemical stainings were first examined with an epifluorescence microscope (BX61, Olympus) equipped with the appropriate filter sets. Stainings were further analyzed with a LSM710 laser-scanning confocal microscope (Carl Zeiss,). Digital images were captured using the ZEN software (Carl Zeiss).

We performed timelapse microscopy to follow the reprogramming process of pericytes into iNs. Pericytes were transduced with Ascl1-Sox2-CAG-GFP retrovirus. 24 h following transduction, medium was replaced by a differentiation medium consisting of DMEM high glucose with GlutaMAX and B27 supplement (Gibco). The microwell plate containing these cells was 48 h later placed on a heated microscopic stage with 5% CO2 and 37°C and imaged continuously for up to 14 days. Fluorescent images were taken subsequently once

every 4 hours and bright field images once every 5 minutes. After completion of timelapse imaging, cells were fixed with 4% PFA and post imaging ICC was performed to corroborate the results from the imaging. Data analysis was performed using Timm's Tracking Tool (TTT) software.

Sholl analysis

Sholl analysis was performed by using the ImageJ plugin *Sholl Analysis*44. Confocal images of iNs with immunocytochemical stainings against TUBB3 were used for tracing individual neuronal processes of selected cells in ImageJ (Fiji) software 45. After assigning the center of each cell soma, a grid with concentric circles with increasing diameter (5 μm) was superimposed. The data are expressed as the mean ± SEM of the values obtained in four independent experiments; untreated n = 14, Dorsomorphin-treated n = 14. The investigators carried out blinded analyses.

Neuromorphometry

Several parameters of cell morphology were examined. Neuronal complexity quantification was conducted with the following measurements: (1) Primary branches - processes emerging directly from the soma per neuron; (2) Dendritic segment - part of the dendrite between two branching points; (3) Branching point - point at the dendrite where a dendrite ramifies into two or more; (4) Maximum dendritic length or ending radius - the radius of the largest circle of the superimposed Sholl mask; (5) Soma size (μm2) - cross sectional surface area of the cell body; (6) Sum of intersections - the sum of all intersections between the dendritic arbors and the concentric circles radiating from the cell body. The number of primary branches, as well as the number of dendritic segments and branching points were counted manually. ImageJ Fiji software was used to measure soma size. The sum of intersections and the ending radius were measured by using the Sholl method (see Sholl Analysis).

Statistics

To test for statistical significance, two-tailed unpaired Student's t test was used. Asterisks indicate statistically significant differences across the two group, $*P < 0.05$, $**P < 0.01$, $***P < 0.001$. The analyses were done using Prism (GraphPad) or R. Data distribution was assumed to be normal but this was not formally tested. Throughout the study boxplots show median, quartiles (box), and range (whiskers). No statistical methods were used to pre-determine sample sizes but our sample sizes are similar to those reported in previous publications 11,16. If not indicated otherwise, data collection and analysis were not performed blind to the conditions of the experiments. No data points were excluded for the analysis, except for cells in the scRNA-seq analyses not fulfilling the required criteria (see below sections on scRNA-seq analyses). The information concerning sample sizes, randomization, data exclusion etc. can also be found in the "Life Science Reporting Summary".

Electrophysiology

For electrophysiological recordings, coverslips with reprogrammed cells were transferred to a recording chamber mounted on the stage of an upright microscope (Axioscope FS, Zeiss,

Germany). Cells were perfused with a bathing solution consisting of (in mM): NaCl 150, KCl 3, CaCl2 3, MgCl2 2, 4-(2-hydroxyethyl)-1-piperazineethanesulfonic acid (HEPES) 10, and D-glucose 10. The pH of the solution was adjusted to 7.4 (NaOH); the osmolarity ranged between 309 to 313 mOsmol. All recordings were performed at room temperature (23 – 24°C). The electrodes for whole cell patch-clamp recordings were fabricated from borosilicate glass capillaries (OD: 1.5 mm, ID: 0.86 mm, Hugo Sachs Elektronik-Harvard Apparatus) and filled with a solution composed of (in mM): potassium gluconate 135, KCl 4, NaCl 2, ethylene glycol-bis(2-aminoethylether)-N,N,N′,N′-tetraacetic acid (EGTA) 0.2, HEPES (potassium salt) 10, adenosine-triphosphate (magnesium salt, ATP[Mg]) 4, sodium guanosine-triphosphate (NaGTP) 0.5, and phosphocreatine 10 (pH: 7.25 – 7.30, osmolarity: 288 – 291 mOsmol). The electrodes (resistance: 5 – 7 MΩ) were connected to the headstage of a npi ELC-03XS amplifier (npi, Tamm, Germany). In order to visualize the cultured cells, the microscope was equipped with differential interference contrast (DIC) optics and with epifluorescence optics for green and red fluorescence (filter sets: Zeiss BP450-490, LP520, Zeiss BP546/12, lP590). Images were taken and displayed using a software-operated CCD microscope camera (ORCA R, Hamamatsu, Germany). Following membrane rupture, the cells were voltage-clamped to a holding potential of -60 mV and kept under this condition until stabilization of the holding current was achieved (3 – 5 min). Then the amplifier was switched to the current-clamp mode. The recorded signals were amplified (x10), filtered at 10 or 20 kHz (current clamp) and 5 kHz (voltage clamp), digitized at a sampling rate of 10 or 20 kHz and stored on a computer for off-line analysis. Data acquisition and generation of command pulses was done by means of a CED 1401 Micro 3 system in conjunction with Signal6 data acquisition software (Cambridge electronic design). Data analysis was performed using IGOR Pro 6 (WaveMetrics, Lake Oswego, USA) together with the NeuroMatic IGOR plugin (www.neuromatic.thinkrandom.com). Determination of the input resistance RN was performed by measurement of the amplitude of a voltage deviation induced by a small hyperpolarizing current pulse (1 s, 2 – 10 pA). The total membrane capacity CN was estimated using a method described by (Zemankovics et al., 2010). The ability of the cells to generate action potentials was tested by injecting depolarizing current pulses (50 ms) with increasing current strengths (ΔI: 2 - 10 pA) or by depolarizing current ramps (50 ms) from 0 – 100 pA. Spike discharge was analyzed by injecting a series of depolarizing current pulses (duration: 1 s) with a stepwise increment (ΔI: 2 - 10 pA).

Bulk RNA-sequencing

Primary pericytes of 3 different human donors were transduced with either Ascl1, Sox2, AS, and control retroviruses and purified by FAC sorting at 2 and 7 dpi. RNA was isolated using the RNeasy Micro Kit (Qiagen). Following Ribo-Zero removal RNA-seq library was prepared in accordance with Illumina's instructions using oligo-dT primers. The RNAseq output in FASTQ format was aligned to human hg38 genome (sourced from UCSC) using TopHat v2.0.846 and only uniquely mapped reads were retained for further analysis. SAMTOOLS v.0.1.1947 was used for file format conversions (SAM and BAM). The read counts per gene was calculated using the HTSeq program, v0.5.4p148. The DESeq49 package was used thereafter for differential expression analysis. The padj value was calculated with the Benjamini-Hochberg procedure.

GO terms analysis of bulk RNA-seq data

GO enrichment analysis was performed using the Bioconductor package TopGO employing the default algorithm *weight01*50. Genes were considered significantly deregulated with a padj<0.01. GO terms were ordered according to their significance as determined by Fisher´s exact test.

Capturing of single cells and preparation of cDNA

Transduced human brain pericytes were sorted using FACS and single cells were captured on a medium-sized (10–17 μ m cell diameter) microfluidic RNA-seq chip using the Fluidigm C1 system. Cells were loaded onto the chip at a concentration of 350–500 cells per μl and imaged by phase-contrast to assess number of cells per capture site. Only single cells were included in the analysis. cDNAs were prepared on chip using the SMARTer v4 Ultra Input Low RNA kit for Illumina (Clontech).

RNA-seq library construction and cDNA sequencing

Size distribution and concentration of single-cell cDNA was assessed on a capillary electrophoresis based fragment analyser (Advanced Analytical Technologies) and only single cells with high quality cDNA were further processed. Sequencing libraries were constructed in 96-well plates using the Illumina Nextera XT DNA Sample Preparation kit using primer sets A and B according to the protocol supplied by Fluidigm and as described previously11. Libraries were quantified by Agilent Bioanalyzer using High Sensitivity DNA analysis kit as well as fluorometrically using Qubit dsDNA HS Assay kits and a Qubit 2.0 Fluorometer (Invitrogen, Thermo Fisher Scientific). Up to 192 single-cell libraries were pooled and sequenced 100 bp paired-end on one lane of Illumina HiSeq 2500 to a depth of at least 500,000 reads per cell. Basecalling, adaptor trimming, and de-multiplexing was performed as described51,52. The transcriptome of a total of 769 cells was measured from the following 12 independent experiments: d2 control (76 cells, 1 experiment), d2 Ascl1-only (82 cells, 1 experiment, d7 Ascl1-only (64 cells, 1 experiment), d2 AS (86 cells, 1 experiment), d7 AS (48 cells, 1 experiment), d14 AS (79 cells, 2 experiments), d21/22 AS (130 cells, 2 experiments), d14 ASD (183 cells, 2 experiments), d14 ASN (21 cells, 1 experiment). See Supplementary Table 5 for the transcriptome data for all 769 cells with annotations (quantification in log2[FPKM]).

Processing, analysis and graphic display of single cell RNA-seq data

Reads were aligned to a Bowtie253 indexed human genome (hg38 sourced from Ensembl) supplemented with DNA sequences for *Egfp, mCherry, DsRed*, mouse *Ascl1*, and mouse *Sox2* using TopHat46 with default settings. Transcript levels were quantified as Fragments Per Kilobase of Mapped reads (FPKM) generated by Cufflinks54 using gencode protein coding genes (hg38 Havana). We excluded cells that had less than 100,000 reads, did not express > 1000 genes, or did not express either of two housekeeping genes *ACTB* and *GAPDH*. Transcript levels were converted to the log-space by taking the log2 (FPKM). R studio (https://www.rstudio.com/) was used to run custom R scripts to perform principal component analysis (PCA, FactoMineR package), hierarchical clustering (stats package) and to construct heatmaps, correlation plots, scatter plots, violin plots, dendrograms, bar graphs,

Europe PMC Funders Author Manuscripts

and histograms. Generally, ggplot2 and gplots packages were used to generate data graphs. The Seurat package implemented in R was used to identify cell clusters and perform differential gene expression based on tSNE55. The Monocle2 package20 was used to analyze cell lineage relationships. Covariance network analysis and visualizations were done using igraph implemented in R (http://igraph.sf.net). Signatures were calculated by summing the log2 FPKM expression values of each gene in a set of genes comprising a signature (Supplementary Table 6)

10x Genomics scRNA-seq experiment

For the 10X Genomics experiment, cells were transfected with AS, treated with Dorsomorphin, and analyzed at 14 dpi. Cells were sorted based on the expression of GFP and used for 1 encapsulation. 10X Genomics sample libraries were sequenced on on an Illumina HiSeq 2500 and base-calling, adaptor trimming, and de-multiplexing of single cells were performed using 10X Genomics Cell Ranger 2.0 software. We performed PCA and tSNE analyses using the Seurat v2.0 package for R on 3,419 single cells with 1,000 – 7,000 genes detected (Supplementary Table 7). We used genes correlating and anti-correlating with the first 8 principal components to cluster the cells, and found that clustering patterns were robust across multiple PC inclusions. Neuronal cluster specific markers were found using Seurat's implementation of the 'bimod' likelihood-ratio test for single cell gene expression data and the top genes were selected based on the average log fold change.

Antibodies

Mouse (IgG2b) anti-TUBB3 (Sigma; cat.no. T8660; 1:300), rat IgG2a anti-CD49f-PE (Miltenyi Biotec; cat.no. 130-100-096; 1:11), recombinant human anti-CD4 (Miltenyi; cat.no. 130-109-537; 1:11), rabbit anti-GABA (Abcam; cat.no. ab17413; 1:1000), chick anti-GFP (Aves; cat.no. GFP-1020; 1:500), mouse (IgG1) anti-Pvalb (Swant; cat.no. PV-235; 1:1000), rabbit anti-Pdgfrb (Cell Signaling; cat.no. 3169S; 1:300), rat anti-RFP (Chromotek; cat.no. 5F8; 1:500), mouse (IgG2b) anti-SMA (Sigma; cat.no. A5228; 1:500), rabbit anti-VGLUT1 (Synaptic Systems, cat.no. 135302; 1:500). For FACS: mouse (IgG2b) anti-LEPR Al647 (BD Pharmingen; cat.no. 564376; 1:20), corresponding isotype control (BD Pharmingen; cat.no. 557903; 1:20). Antibodies were selected according to the antibody validation reported by the distributing companies.

Supplementary Material

Refer to Web version on PubMed Central for supplementary material.

Acknowledgement

We thank M Wernig (Stanford University) for generously providing us with the Sox2 coding sequence. We are also very grateful to B. Sutor (BMC, LMU Munich) for help with the electrophysiological experiments, R. Menon (UMC Mainz) for help with the cell culture experiments, A. Bosio (Miltenyi Biotec) for help with the multidimensional fluorescence stainings, and F. Calzolari (UMC Mainz) for comments on the manuscript. We thank B. Höber, A. Weihmann, J. Kelso of MPI-EVA for sequencing and bioinformatics support with this project. Flow cytometric cell sorting was performed at the "Core Unit Durchflusszytometrie" (CUDZ) of the Cente for Infectious Diseases at the College of Veterinary Medicine, University of Leipzig, Leipzig, Germany. S.F. was supported by a fellowship from the Swiss National Science Foundation (PA00P3_139709). W.F. was supported by a Fellowship from the China Research Council. This work was supported by the following grants: advanced ERC ChroNeuroRepair to M.G.; Bavarian State Ministry of Sciences, Research and the Arts to M.K. and B.B. (ForIPS

D2-F2412.26); Schram foundation (T287/29577/2017) and Wings For (WFL-DE-012/14) Life to M.K.; Max Planck Society to B.T.; DFG (INST 161/875-2; BE 4182/8-1), NEURON ERA-NET (01EW1604), and Wellcome Trust (206410/Z/17/Z) to B.B.

References

1. Heinrich C, Spagnoli FM, Berninger B. In vivo reprogramming for tissue repair. Nat Cell Biol. 2015; 17:204–211. DOI: 10.1038/ncb3108 [PubMed: 25720960]
2. Amamoto R, Arlotta P. Development-inspired reprogramming of the mammalian central nervous system. Science. 2014; 343doi: 10.1126/science.1239882
3. Mertens J, Marchetto MC, Bardy C, Gage FH. Evaluating cell reprogramming, differentiation and conversion technologies in neuroscience. Nat Rev Neurosci. 2016; 17:424–437. DOI: 10.1038/nrn.2016.46 [PubMed: 27194476]
4. Srivastava D, DeWitt N. In Vivo Cellular Reprogramming: The Next Generation. Cell. 2016; 166:1386–1396. DOI: 10.1016/j.cell.2016.08.055 [PubMed: 27610565]
5. Ruiz S, et al. A high proliferation rate is required for cell reprogramming and maintenance of human embryonic stem cell identity. Curr Biol. 2011; 21:45–52. DOI: 10.1016/j.cub.2010.11.049 [PubMed: 21167714]
6. Morris SA. Direct lineage reprogramming via pioneer factors; a detour through developmental gene regulatory networks. Development. 2016; 143:2696–2705. DOI: 10.1242/dev.138263 [PubMed: 27486230]
7. Vierbuchen T, Wernig M. Molecular roadblocks for cellular reprogramming. Mol Cell. 2012; 47:827–838. DOI: 10.1016/j.molcel.2012.09.008 [PubMed: 23020854]
8. Gascon S, Masserdotti G, Russo GL, Gotz M. Direct Neuronal Reprogramming: Achievements, Hurdles, and New Roads to Success. Cell Stem Cell. 2017; 21:18–34. DOI: 10.1016/j.stem.2017.06.011 [PubMed: 28686866]
9. Wapinski OL, et al. Hierarchical mechanisms for direct reprogramming of fibroblasts to neurons. Cell. 2013; 155:621–635. DOI: 10.1016/j.cell.2013.09.028 [PubMed: 24243019]
10. Masserdotti G, et al. Transcriptional Mechanisms of Proneural Factors and REST in Regulating Neuronal Reprogramming of Astrocytes. Cell Stem Cell. 2015; 17:74–88. DOI: 10.1016/j.stem.2015.05.014 [PubMed: 26119235]
11. Treutlein B, et al. Dissecting direct reprogramming from fibroblast to neuron using single-cell RNA-seq. Nature. 2016; 534:391–395. DOI: 10.1038/nature18323 [PubMed: 27281220]
12. Mall M, et al. Myt1l safeguards neuronal identity by actively repressing many non-neuronal fates. Nature. 2017; doi: 10.1038/nature21722
13. Heinrich C, et al. Directing astroglia from the cerebral cortex into subtype specific functional neurons. PLoS Biol. 2010; 8doi: 10.1371/journal.pbio.1000373
14. Chanda S, Marro S, Wernig M, Sudhof TC. Neurons generated by direct conversion of fibroblasts reproduce synaptic phenotype caused by autism-associated neuroligin-3 mutation. Proc Natl Acad Sci U S A. 2013; 110:16622–16627. DOI: 10.1073/pnas.1316240110 [PubMed: 24046374]
15. Vierbuchen T, et al. Direct conversion of fibroblasts to functional neurons by defined factors. Nature. 2010; 463:1035–1041. DOI: 10.1038/nature08797 [PubMed: 20107439]
16. Karow M, et al. Reprogramming of pericyte-derived cells of the adult human brain into induced neuronal cells. Cell Stem Cell. 2012; 11:471–476. DOI: 10.1016/j.stem.2012.07.007 [PubMed: 23040476]
17. Long JE, et al. Dlx1&2 and Mash1 transcription factors control striatal patterning and differentiation through parallel and overlapping pathways. J Comp Neurol. 2009; 512:556–572. DOI: 10.1002/cne.21854 [PubMed: 19030180]
18. Liu SJ, et al. Single-cell analysis of long non-coding RNAs in the developing human neocortex. Genome Biol. 2016; 17:67.doi: 10.1186/s13059-016-0932-1 [PubMed: 27081004]
19. Raposo AA, et al. Ascl1 Coordinately Regulates Gene Expression and the Chromatin Landscape during Neurogenesis. Cell Rep. 2015; doi: 10.1016/j.celrep.2015.02.025

Europe PMC Funders Author Manuscripts

20. Trapnell C, et al. The dynamics and regulators of cell fate decisions are revealed by pseudotemporal ordering of single cells. Nat Biotechnol. 2014; 32:381–386. DOI: 10.1038/nbt.2859 [PubMed: 24658644]
21. Camp JG, et al. Human cerebral organoids recapitulate gene expression programs of fetal neocortex development. Proc Natl Acad Sci U S A. 2015; 112:15672–15677. DOI: 10.1073/pnas.1520760112 [PubMed: 26644564]
22. Suzuki IK, Vanderhaeghen P. Is this a brain which I see before me? Modeling human neural development with pluripotent stem cells. Development. 2015; 142:3138–3150. DOI: 10.1242/dev.120568 [PubMed: 26395142]
23. Imayoshi I, Sakamoto M, Yamaguchi M, Mori K, Kageyama R. Essential roles of Notch signaling in maintenance of neural stem cells in developing and adult brains. J Neurosci. 2010; 30:3489–3498. DOI: 10.1523/JNEUROSCI.4987-09.2010 [PubMed: 20203209]
24. Guillemot F. Spatial and temporal specification of neural fates by transcription factor codes. Development. 2007; 134:3771–3780. DOI: 10.1242/dev.006379 [PubMed: 17898002]
25. Ladewig J, et al. Small molecules enable highly efficient neuronal conversion of human fibroblasts. Nat Methods. 2012; 9:575–578. DOI: 10.1038/nmeth.1972 [PubMed: 22484851]
26. Dias Moura Prazeres PH, et al. Pericytes are heterogeneous in their origin within the same tissue. Dev Biol. 2017; 427:6–11. DOI: 10.1016/j.ydbio.2017.05.001 [PubMed: 28479340]
27. La Manno G, et al. Molecular Diversity of Midbrain Development in Mouse, Human, and Stem Cells. Cell. 2016; 167:566–580 e519. DOI: 10.1016/j.cell.2016.09.027 [PubMed: 27716510]
28. Goritz C, et al. A pericyte origin of spinal cord scar tissue. Science. 2011; 333:238–242. DOI: 10.1126/science.1203165 [PubMed: 21737741]
29. Chambers SM, et al. Highly efficient neural conversion of human ES and iPS cells by dual inhibition of SMAD signaling. Nat Biotechnol. 2009; 27:275–280. DOI: 10.1038/nbt.1529 [PubMed: 19252484]
30. Liu ML, et al. Small molecules enable neurogenin 2 to efficiently convert human fibroblasts into cholinergic neurons. Nat Commun. 2013; 4doi: 10.1038/ncomms3183
31. Kageyama R, Ohtsuka T, Shimojo H, Imayoshi I. Dynamic regulation of Notch signaling in neural progenitor cells. Curr Opin Cell Biol. 2009; 21:733–740. DOI: 10.1016/j.ceb.2009.08.009 [PubMed: 19783418]
32. Vasconcelos FF, et al. MyT1 Counteracts the Neural Progenitor Program to Promote Vertebrate Neurogenesis. Cell Rep. 2016; 17:469–483. DOI: 10.1016/j.celrep.2016.09.024 [PubMed: 27705795]
33. Engler A, et al. Notch2 Signaling Maintains NSC Quiescence in the Murine Ventricular-Subventricular Zone. Cell Rep. 2018; 22:992–1002. DOI: 10.1016/j.celrep.2017.12.094 [PubMed: 29386140]
34. Radonjic NV, et al. Diversity of cortical interneurons in primates: the role of the dorsal proliferative niche. Cell Rep. 2014; 9:2139–2151. DOI: 10.1016/j.celrep.2014.11.026 [PubMed: 25497090]
35. Karow M, Schichor C, Beckervordersandforth R, Berninger B. Lineage-reprogramming of pericyte-derived cells of the adult human brain into induced neurons. J Vis Exp. 2014; doi: 10.3791/51433
36. Yu PB, et al. Dorsomorphin inhibits BMP signals required for embryogenesis and iron metabolism. Nat Chem Biol. 2008; 4:33–41. DOI: 10.1038/nchembio.2007.54 [PubMed: 18026094]
37. Inman GJ, et al. SB-431542 is a potent and specific inhibitor of transforming growth factor-beta superfamily type I activin receptor-like kinase (ALK) receptors ALK4, ALK5, and ALK7. Mol Pharmacol. 2002; 62:65–74. [PubMed: 12065756]
38. Laping NJ, et al. Inhibition of transforming growth factor (TGF)-beta1-induced extracellular matrix with a novel inhibitor of the TGF-beta type I receptor kinase activity: SB-431542. Mol Pharmacol. 2002; 62:58–64. [PubMed: 12065755]
39. Martynoga B, et al. Epigenomic enhancer annotation reveals a key role for NFIX in neural stem cell quiescence. Genes Dev. 2013; 27:1769–1786. DOI: 10.1101/gad.216804.113 [PubMed: 23964093]

40. Graham A, Francis-West P, Brickell P, Lumsden A. The signalling molecule BMP4 mediates apoptosis in the rhombencephalic neural crest. Nature. 1994; 372:684–686. DOI: 10.1038/372684a0 [PubMed: 7990961]
41. Chen AE, Borowiak M, Sherwood RI, Kweudjeu A, Melton DA. Functional evaluation of ES cell-derived endodermal populations reveals differences between Nodal and Activin A-guided differentiation. Development. 2013; 140:675–686. DOI: 10.1242/dev.085431 [PubMed: 23293299]
42. Kumar A, et al. Nodal signaling uses activin and transforming growth factor-beta receptor-regulated Smads. J Biol Chem. 2001; 276:656–661. DOI: 10.1074/jbc.M004649200 [PubMed: 11024047]
43. Schubert, W. Multiple antigen-mapping microscopy of human tissueExperta Medica Adv Anal Cell Pathol. Burger, G, Oberholzer, M, Vooijs, GP, editors1990. 97–98.
44. Ferreira TA, et al. Neuronal morphometry directly from bitmap images. Nat Methods. 2014; 11:982–984. DOI: 10.1038/nmeth.3125 [PubMed: 25264773]
45. Schindelin J, et al. Fiji: an open-source platform for biological-image analysis. Nat Methods. 2012; 9:676–682. DOI: 10.1038/nmeth.2019 [PubMed: 22743772]
46. Trapnell C, Pachter L, Salzberg SL. TopHat: discovering splice junctions with RNA-Seq. Bioinformatics. 2009; 25:1105–1111. DOI: 10.1093/bioinformatics/btp120 [PubMed: 19289445]
47. Li H, et al. The Sequence Alignment/Map format and SAMtools. Bioinformatics. 2009; 25:2078–2079. DOI: 10.1093/bioinformatics/btp352 [PubMed: 19505943]
48. Anders S, Pyl PT, Huber W. HTSeq--a Python framework to work with high-throughput sequencing data. Bioinformatics. 2015; 31:166–169. DOI: 10.1093/bioinformatics/btu638 [PubMed: 25260700]
49. Oshlack A, Robinson MD, Young MD. From RNA-seq reads to differential expression results. Genome Biol. 2010; 11:220.doi: 10.1186/gb-2010-11-12-220 [PubMed: 21176179]
50. Alexa A, Rahnenfuhrer J, Lengauer T. Improved scoring of functional groups from gene expression data by decorrelating GO graph structure. Bioinformatics. 2006; 22:1600–1607. DOI: 10.1093/bioinformatics/btl140 [PubMed: 16606683]
51. Renaud G, Kircher M, Stenzel U, Kelso J. freeIbis: an efficient basecaller with calibrated quality scores for Illumina sequencers. Bioinformatics. 2013; 29:1208–1209. DOI: 10.1093/bioinformatics/btt117 [PubMed: 23471300]
52. Renaud G, Stenzel U, Maricic T, Wiebe V, Kelso J. deML: robust demultiplexing of Illumina sequences using a likelihood-based approach. Bioinformatics. 2015; 31:770–772. DOI: 10.1093/bioinformatics/btu719 [PubMed: 25359895]
53. Langmead B, Salzberg SL. Fast gapped-read alignment with Bowtie 2. Nat Methods. 2012; 9:357–359. DOI: 10.1038/nmeth.1923 [PubMed: 22388286]
54. Trapnell C, et al. Transcript assembly and quantification by RNA-Seq reveals unannotated transcripts and isoform switching during cell differentiation. Nat Biotechnol. 2010; 28:511–515. DOI: 10.1038/nbt.1621 [PubMed: 20436464]
55. Macosko EZ, et al. Highly Parallel Genome-wide Expression Profiling of Individual Cells Using Nanoliter Droplets. Cell. 2015; 161:1202–1214. DOI: 10.1016/j.cell.2015.05.002 [PubMed: 26000488]

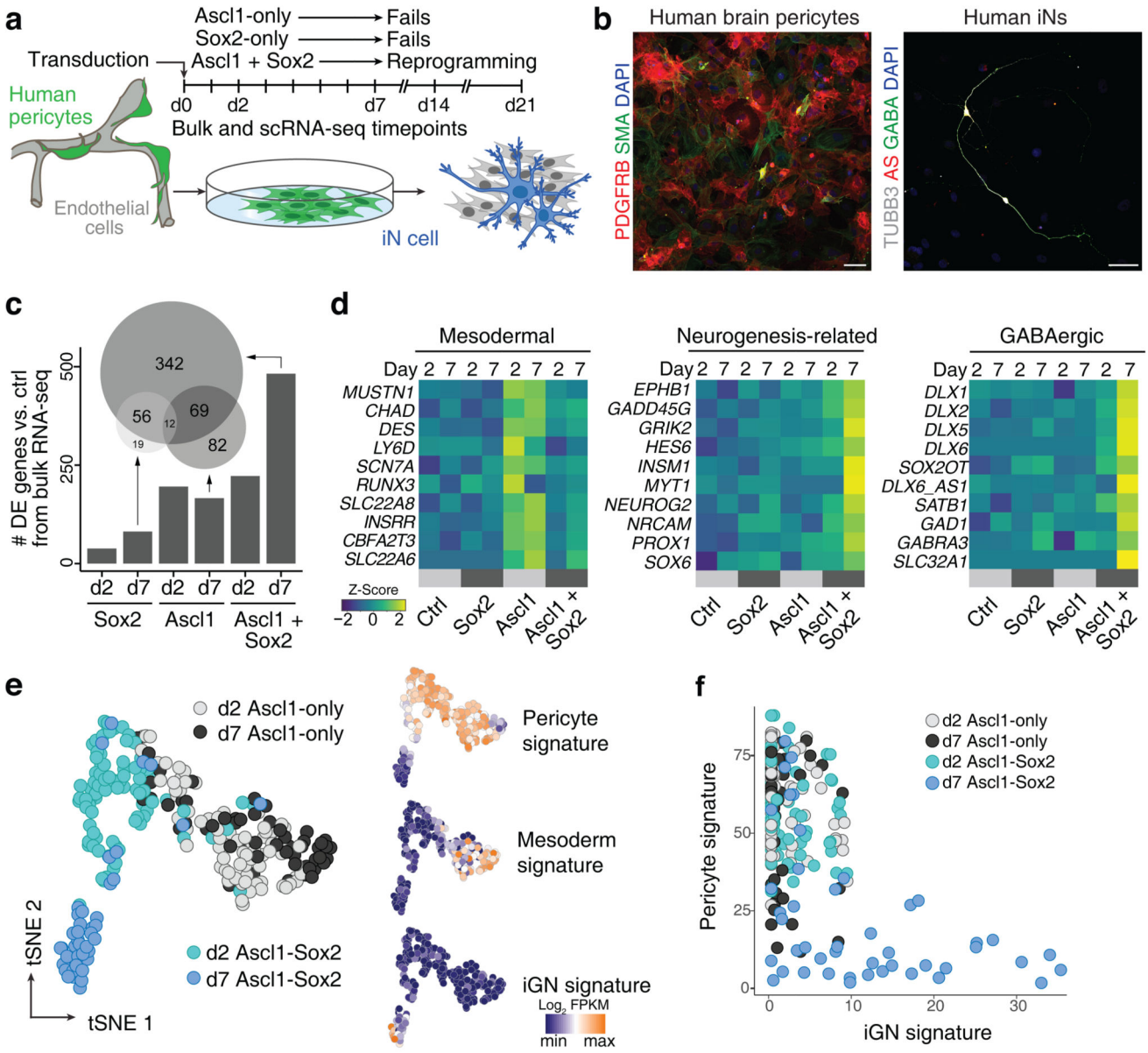

Fig. 1. Ascl1-Sox2 synergism is required for pericyte-to-iN reprogramming.

a, Schematic of experiments in this figure. Cells expressing Ascl1 and/or Sox2 are fluorescently labeled and isolated by FACS for bulk and scRNA-seq analyses at indicated time points following transduction. **b,** Representative micrographs of cultured human pericytes expressing pericyte markers PDGFRB and SMA, before (left) and after transformation (right) into TUBB3- and GABA-positive induced neurons by overexpressing AS at 46 dpi (n >30). Nuclei are stained with Dapi. Scale bar = 50 μm. **c,** Bulk RNA-seq with pericytes derived from three individual donors was performed at 2 and 7 dpi with Ascl1-only, Sox2-only, or Ascl1 + Sox2 (AS). Bar graph shows the number of differentially expressed (DE) genes (padj < 0.01; calculated according to Benjamini-Hochberg) in each condition compared to pericytes transduced with a control vector. The Euler diagram shows

Europe PMC Funders Author Manuscripts

the overlap of the DE genes at 7 dpi. Note that the majority of the DE genes results from AS synergism. **d,** Heatmaps show normalized expression (Z-score) of representative DE genes highlighting the induction of mesodermal, neurogenesis-related, and GABAergic signature genes at both 2 and 7 dpi. **e,** ScRNA-seq was performed 2 and 7 dpi on cells transduced with Ascl1-only (2 dpi 82 cells; 7 dpi 64 cells) and AS (2 dpi 86 cells; 7 dpi 48 cells). PCA (calculated on a total of 280 cells) followed by tSNE shows that the pericyte signature is diminished in many d7 Ascl1-only and strongly diminished in the majority of d7 AS cells, concomitant with the acquisition of a mesoderm and iGN signature in Ascl1-only and AS- cells, respectively. Signatures were calculated by summing the expression of the fate-determinants highlighted in panels d (Supplementary Table 5). **f,** The iGN signature is plotted for all Ascl1-only and AS cells relative to the pericyte signature.

Europe PMC Funders Author Manuscripts

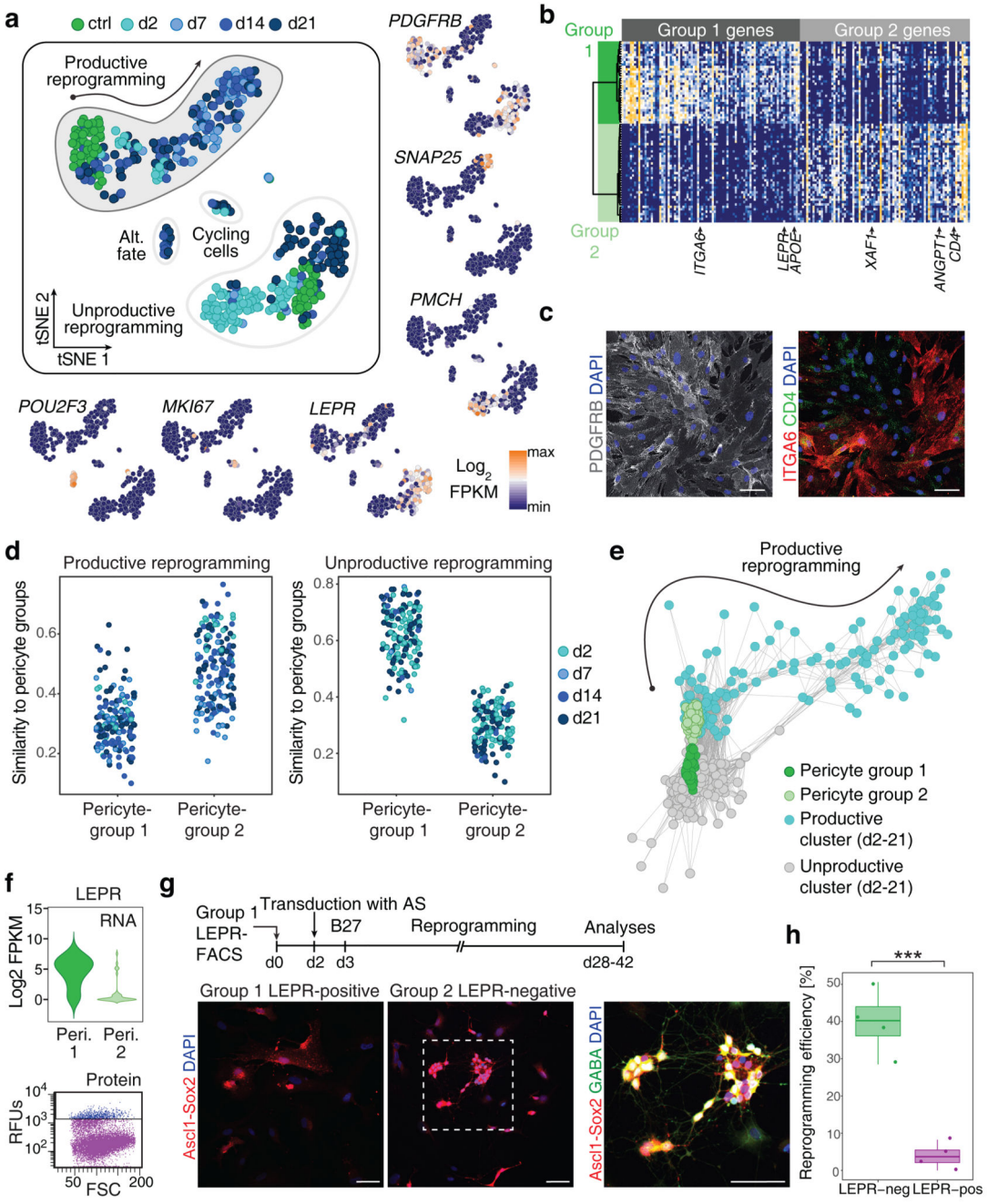

Fig. 2. Pericyte heterogeneity correlates with distinct reprogramming competence.

a, PCA (total of 419 cells) followed by tSNE reveals heterogeneity during iN reprogramming, with genes marking distinct clusters colored on the adjacent tSNE plots. Control-transduced pericytes (green) segregate into two distinct clusters. One cluster links to cells that express iN fate determinants (productive), whereas the other cluster is unlinked to iN reprogramming (unproductive). Cells expressing *MKI67* and other hallmarks of cycling cells are observed, as well as a group of cells expressing *POU2F3*. **b,** Heatmap shows the expression of genes that correlate with PC1 from PCA on control-pericytes only.

Europe PMC Funders Author Manuscripts

Hierarchical clustering reveals two distinct groups of pericytes with selected genes indicated below the heatmap. **c,** Micrographs showing cultured human brain pericytes stained against pan-pericyte marker PDGFRB (left panel). Right panel shows the same field of view of cultured human brain pericytes stained against pericyte group 1 marker ITGA6 and pericyte group 2 marker CD4. Nuclei are stained with Dapi (n = 3 individual pericyte donors; two independent experiments). Scale bar = 50 μm. **d,** Cells from the productive reprogramming cluster in Fig. 2a have a higher similarity to group 2 pericytes while cells from the unproductive reprogramming clusters have a higher similarity to group 1 pericytes. **e,** Lineage network based on pairwise correlations between cells suggests that group 2 pericytes (lighter green population) are more competent to contribute to productive iN reprogramming. **f,** Violin blots show the density distribution of RNA expression of *LEPR* in pericyte groups 1 (31 cells) and 2 (44 cells) (upper panel). Representative flow cytometry plots show the protein expression of LEPR in cultured human brain pericytes (lower panel; 4 independent experiments). **g,** Human brain pericytes were sorted based on LEPR expression (group 1 marker), plated and transduced with AS to induce lineage conversion. Micrographs show AS-transduced pericytes at 35 dpi, with inset showing higher magnification of reprogrammed pericytes that acquired neuronal morphology and GABA immunoreactivity (n = 4). Nuclei are stained with Dapi. Scale bars = 50 μm. **h,** Quantification of reprogramming efficiency (dots represent independent individual experiments; n = 4; data are represented as boxplots with whiskers; two-tailed unpaired Student's t test; P = 0,000593; ***$P < 0.001$; boxplots show median, quartiles (box), and range (whiskers)) reveals that the LepR-negative pericyte subpopulation is more competent to iN reprograming using AS, confirming predictions from scRNA-seq.

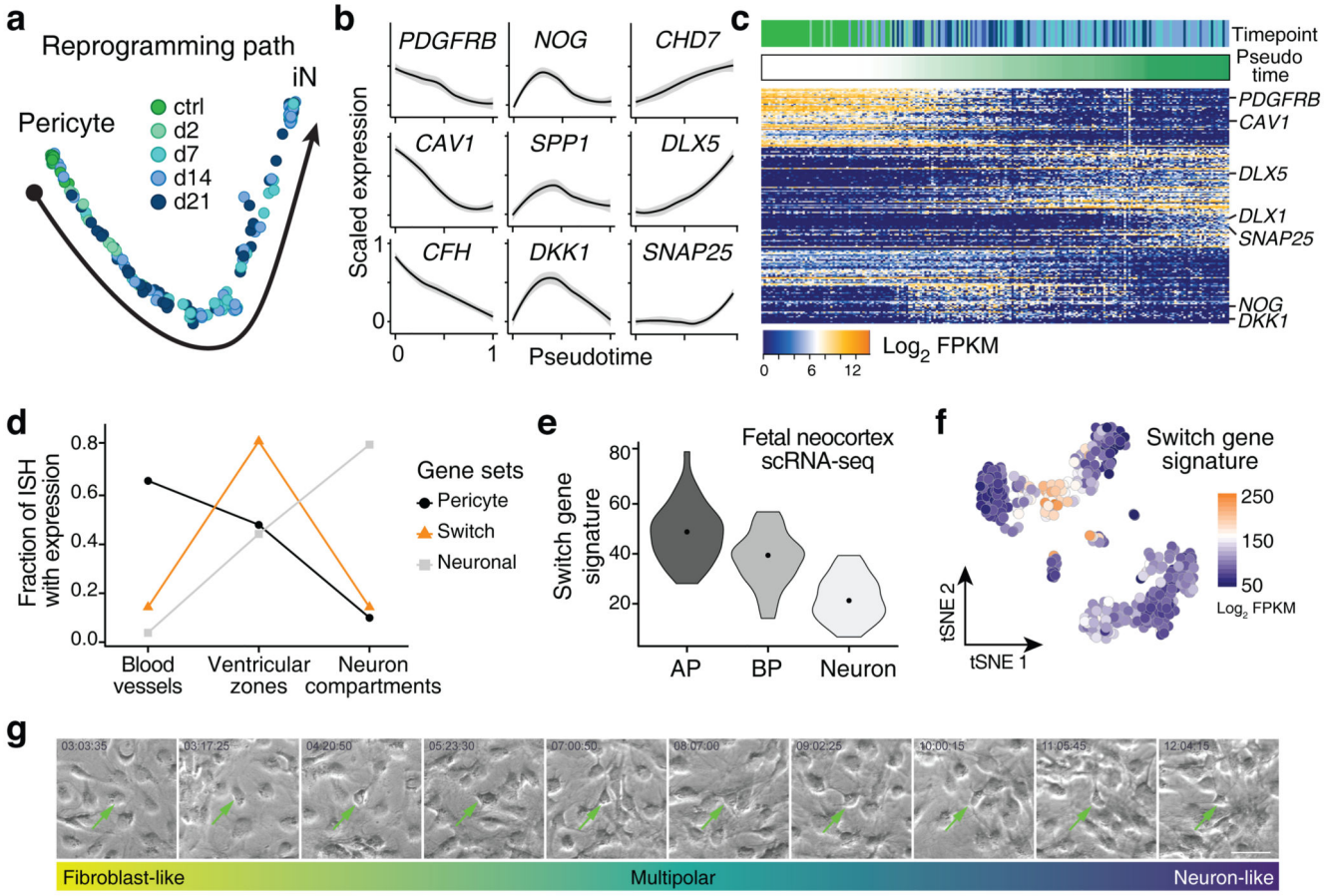

Fig. 3. A transient neural precursor-like state emerges on the reprogramming path to iNs.

a, PCA was performed on 211 single cell transcriptomes from the productive reprogramming cluster from Fig. 2a. Monocle2 was used to infer a pseudotemporal ordering of cells. **b,** Scaled expression of representative marker genes in all 211 cells of the productive reprogramming path shown as a function of pseudotime. Shaded gray represents 0.95 confidence interval. **c,** Heatmap shows the expression of genes identified by PCA and ordered by hierarchical clustering. Cells are ordered according to pseudotime. The reprogramming path is characterized by three phases of gene expression changes. In the first phase, genes associated with pericyte identity are down-regulated concomitant with a transient upregulation of switch genes (e.g. *NOG, DKK1*). In a second phase, genes associated with iN fate determination are upregulated (e.g. *DLX5*). In a third phase, neuron maturation factors (e.g. *DLX1, SNAP25*) are upregulated alongside phase 2 genes. **d,** Chart shows fraction of pericyte, switch, and neuronal genes (from panel c) expressed in bloodvessels/meninges, ventricular zones, or neuron compartments determined from in situ patterns in the developing mouse brain. **e,** Violin plots show the density distribution of the switch gene signature from scRNA-seq of fetal human cortex (dots within the violins represent medians). Cortex cells are grouped based on cell type (41 cells apical progenitor, AP; 19 cells basal progenitor, BP; 42 cells early-born neurons, Neuron). **f,** Switch gene signature projected onto tSNE plot from Fig. 2a shows the induction of switch genes at an intermediate stage exclusively within the productive reprogramming path. **g,** Time-lapse

Europe PMC Funders Author Manuscripts

imaging of AS-transduced cells over time (three independent experiments) shows the morphological changes during successful pericyte-to-neuron reprogramming (time points are specified within the pictures). Arrows indicate a successfully reprogrammed pericyte throughout the different morphological changes mentioned below the images. Scale bar = 50 μm.

Europe PMC Funders Author Manuscripts

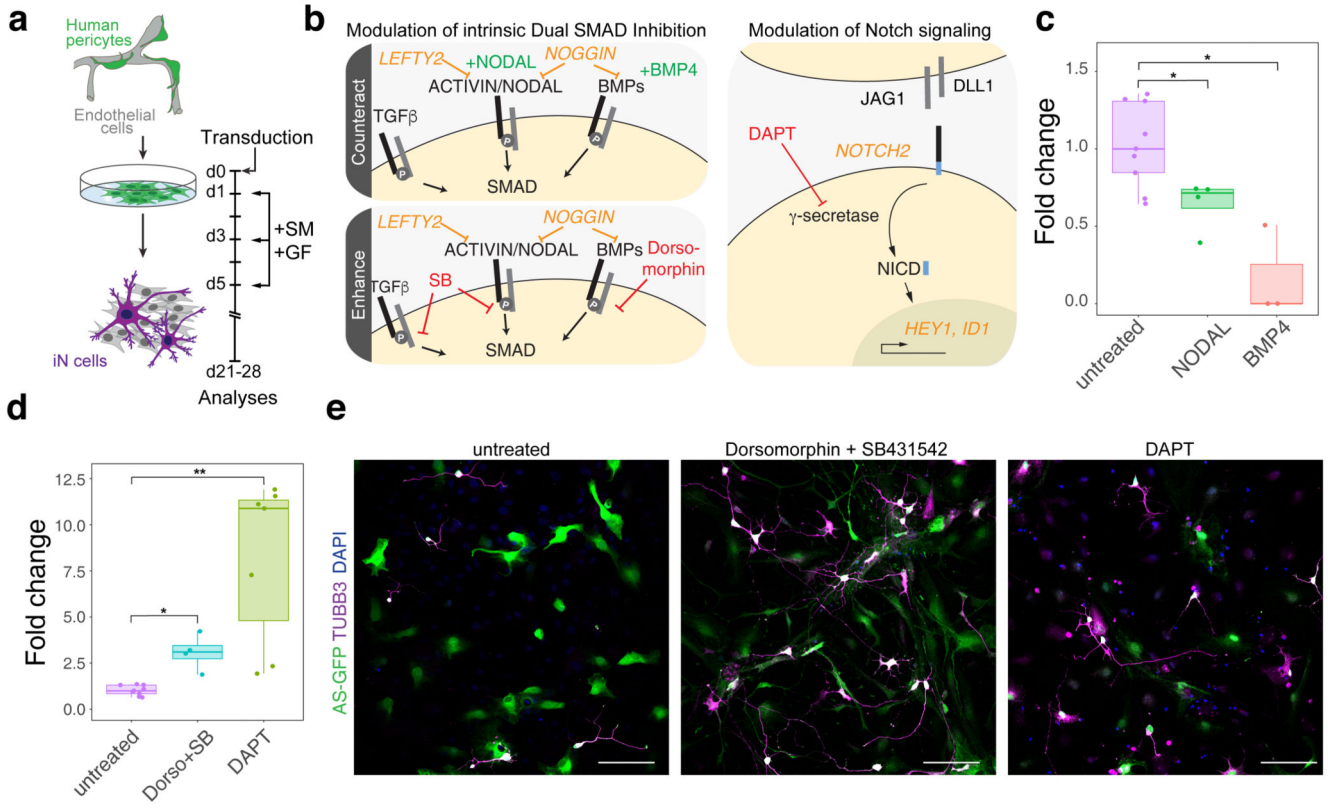

Fig. 4. Modulation of signaling pathways identified during neural stem cell-like state.

a, Schematical overview of the experimental timeline for the experiments contained in this figure. Cell were treated with either small molecules (SM) or growth factors (GF). **b,** Schematic overview of switch gene expression associated with signaling pathways and summary of treatments. **c,** Treatment with NODAL or BMP4 decreases the reprogramming efficiency. Reprogramming efficiency was calculated by quantifying TUBB3-immunoreactive cells out of reporter-positive transduced cells 3-5 weeks following transduction with AS. The fold change was calculated by determining the ratio of growth factor treated versus non treated TUBB3+ and reporter+ per total reporter+ cells of the transduced pericytes (dots represent independent individual experiments; untreated, n = 9; NODAL, n = 4; BMP, n = 3; data are represented as boxplots with whiskers; two-tailed unpaired Student's t test; $P = 0.01202$ for NODAL; $P = 0.01821$ for BMP4; $^{*}P < 0.05$; boxplots show median, quartiles (box), and range (whiskers)). **d,** Reprogramming efficiencies (TUBB3+ and reporter+ per total reporter+) are increased following enhancing treatments with Dorsomorphin (Dorso) + SB431542 (SB) or DAPT. The fold change was calculated by determining the ratio of small molecule treated versus non treated TUBB3+ and reporter+ per total reporter+ cells of the transduced pericytes (dots represent independent individual experiments; untreated, n = 9; Dorso + SB, n = 4; DAPT, n = 7; data are represented as boxplots with whiskers; two-tailed unpaired Student's t test; $P = 0.02133$ for Dorso + SB; $P = 0.0050$ for DAPT; $^{*}P < 0.05$; $^{**}P < 0.01$, boxplots show median, quartiles (box), and range (whiskers)). **e,** Representative micrographs of AS-transduced pericyte cultures (green) and stained with an antibody against TUBB3 (magenta). Note the

Europe PMC Funders Author Manuscripts

increased appearance of reprogrammed pericytes that acquired neuronal morphology following Dorsomorphin + SB (n = 4) and DAPT (n = 7) treatment compared to the untreated cells. Nuclei are stained with Dapi. Scale bars = 50 μm.

Europe PMC Funders Author Manuscripts

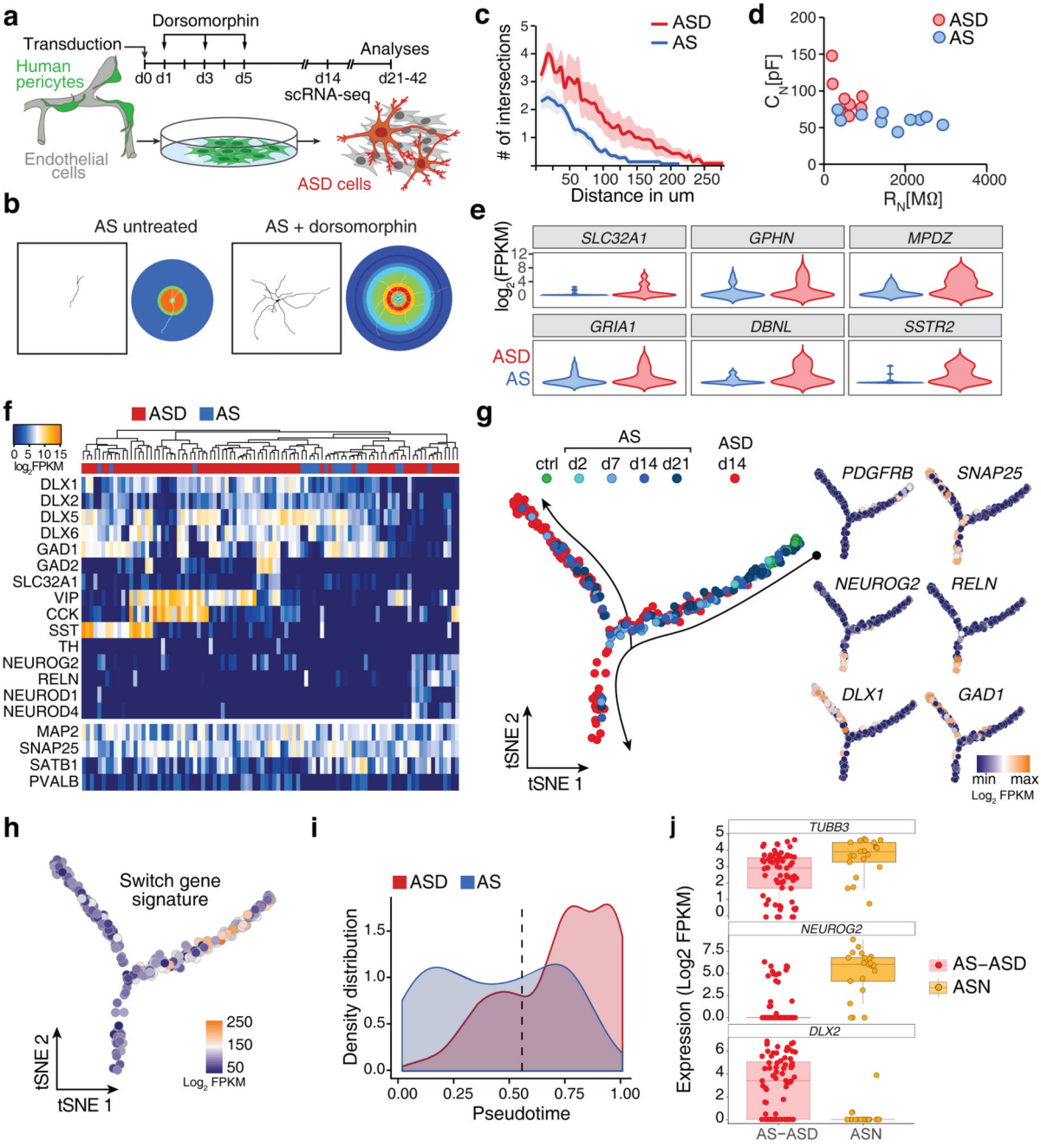

Fig. 5. Pericytes give rise to distinct neuronal subtypes and targeting BMP signaling promotes maturation.

a, Schematical overview of experiments in this figure. **b,** Representative examples of untreated and Dorsomorphin-treated AS-transduced pericytes showing complex branching of dendritic arbors in Dorsomorphin-treated cells. Neuronal morphology was reconstructed using TUBB3 immunoreactivity and used for Sholl analyses. In the Sholl mask (right panels) warmer hues indicate higher number of intersections (untreated, n = 14 cells of 3 independent experiments; Dorsomorphin-treated, n = 14 cells of 3 independent experiments). **c,** Single cell neuromorphology reconstruction by Sholl analysis on

Dorsomorphin treated AS-transduced cells was compared to untreated cells. Note the increase in complexity of Dorsomorphin-treated cells with higher number of intersections with concentric shells and overall increase in the length of the dendrites (see also Supplementary Fig. 4a). Data are represented in a line graph as mean ± SEM (shaded region) (untreated, n = 14 cells of 3 independent experiments; Dorsomorphin-treated, n = 14 cells of 3 independent experiments). **d,** Electrophysiological assessment of AS and ASD cells. Membrane capacitance (CN) is plotted as a function of the membrane resistance (RN). AS cells have larger membrane resistances but smaller membrane capacitances when compared to ASD cells. **e,** Violin blots show the density distribution of expression of selected neuronal maturation genes in neuronal (*SNAP25+, MAP2+, PDGFRB-*) AS (20 cells) and ASD cells (75). **f,** PCA followed by hierarchical clustering was used to characterize neuronal cells (*SNAP25+, MAP2+, PDGFRB-*) AS (20 cells) and ASD cells (75) at 14 dpi regarding the expression of neuronal genes. Note the different interneuron clusters marked by the expression of interneuron subtype-specific genes *VIP, SST*, and *CCK*. **g,** Monocle2 was used to compare maturation of AS and ASD cells. **h,** Switch gene signature from Fig. 3c was projected onto pseudotemporal ordered trancriptomes of Fig. 5g. **i,** The density distributions (i.e. normalized cell number per time point of pseudotime) along the pseudotime of AS transcriptomes (d14) from the productive path and ASD transcriptomes (Fig. 5g) are plotted as function of the distance from the start point. Note the shift of ASD cell transcriptomes compared to AS transcriptomes. The dotted line indicates the bifurcation point in Fig. 5g. **j,** Jitter-boxplot (boxplots show median, quartiles (box), and range (whiskers)) showing the expression of *TUBB3* in all *SNAP25+, MAP2+, PDGFRB-* AS/ASD (71 cells), and ASN (21 cells) cells used for this analysis. Boxplots show the strong increase of *NEUROG2* and decrease in *DLX2* gene expression in ASN cells as compared to AS and ASD cells.

Europe PMC Funders Author Manuscripts